A tris(hydroxymethyl)methyl aminomethane-functionalized SBA-15, SBA-16 and MCM-41 for recovery of boron from salt lake brine

Qinglong Luo[a,b], Lei Liu[c], Ruiqiang Dong[c], Zhongfu Cheng[c], Mingzhe Dong[a], Zhijian Wu[a], Jun Li[a,*], Xueli Huang[b,*]

[a]*Key Laboratory of Comprehensive and Highly Efficient Utilization of Salt Lake Resources, Qinghai Provincial Key Laboratory of Resources and Chemistry of Salt Lakes, Qinghai Institute of Salt Lakes, Chinese Academy of Sciences, Xining, Qinghai 810008, P.R. China, emails: Junli@isl.ac.cn (J. Li), luoql@isl.ac.cn (Q. Luo), dongmingzhe@isl.ac.cn (M. Dong), zjwu@isl.ac.cn (Z. Wu)*
[b]*College of Chemical Engineering, Xinjiang University, Urumqi 830046, P.R. China, email: xuelih@163.com*
[c]*Northwest Oilfield Company Engineering Technology Research Institute, SINOPEC, Urumqi, 830013, P.R. China, emails: liulei001.xbsj@sinopec.com (L. Liu), 395743433@qq.com (R. Dong), 66926670@qq.com (Z. Cheng)*

ABSTRACT

The removal of boron from aqueous solution and the enrichment of boron from salt lake have attracted more attention. In this work, organo-inorganic hybrid mesoporous boron adsorbents were synthesized by tris(hydroxymethyl)methyl aminomethane (TRIS) grafted onto the mesoporous SBA-15, SBA-16 and MCM-41, respectively. And the structures are characterized by infrared, scanning electron microscopy, energy-dispersive X-ray, mapping, X-ray diffraction, point of zero charge, and Marvin laser particle size analyzer. The results showed that TRIS was successfully grafted onto SBA-15, SBA-16, and MCM-41. The adsorption isotherm and adsorption kinetics were best fitted with Langmuir model and pseudo-second-order rate equation, respectively. The adsorption capacity of the three adsorbents was 15.28, 15.70 and 14.17 mg/g, respectively. And the same functional group has little influence on the boron adsorption capacity of different carrier adsorbents of the same type (organosilicon material). These adsorbents have highly selective adsorption of boron, and maintain good lifetime after adsorption–desorption for 5 times, and the dissolution loss rate of SBA-16-TRIS after ten cycles was 0.93%.

Keywords: Boron adsorbents; SBA-15; SBA-16; MCM-41; Tris(hydroxymethyl)methyl aminomethane

1. Introduction

Boron is distributed in rocks, water, salt, springs, oil, water, animals and plants [1,2]. Boron plays an important role in the development of science and technology, growth of animals and plants, and human life [3–5]. Turkey has the world's largest boron reserves, followed by the United States, Russia, Chile and China. In China, there are many types of boron ore with large reserves, but the quality is low. Sedimentary metamorphic ore contains mostly magnesium/iron-boron ore, which is difficult to process, expensive, and inefficient. Therefore, according to the nature of China's boron resources and the status quo of development and exploitation, salt lake boron ore will be more valuable than solid boron ore for development and exploitation. Boron salt lakes in China are mainly distributed in the Qinghai-Tibet Plateau [2]. The utilization of local salt lake resources plays an important role in achieving

---

* Corresponding authors.

sustainable economic development. The methods to extract boron from salt lake brine include chemical precipitation, acidification, solvent extraction, ion exchange and adsorption [6–10]. Among them, the adsorption method is suitable for boron extraction from salt lake brine with low boron content, which has the advantages of high selectivity, good separation efficiency, simple operation, no pollution, recyclability, and low cost [11].

SBA-15 mesoporous molecular sieve has the characteristics of large surface area [12], uniform pore diameter distribution, adjustable pore size, wall thickness, high hydrothermal stability, and non-porous material as highly active catalysts. The mesoporous material SBA-16 is a novel silica material [13] that features a large cage-like cubic-symmetric structure, thicker pore walls, high specific surface area, and thermal stability. MCM-41 is an ordered mesoporous, a novel nanostructured material [14]. It has the properties of pores in an ordered array of hexagons, uniform size, continuous adjustment of pore diameter in the range of 2–10 nm, and large specific surface area. Therefore, these molecular sieves have good prospects for applications in catalysis, adsorption, and separation.

At present, many types of boron adsorbents have been reported in the literature. Polymeric boron adsorbent functionalized with N-methyl-D-glucamine (MG), glucose, trimethylolaminomethane, glycidyl functionalized ethylenediamine/triethylenetetramine and glucose functionalized ethylenediamine/polyethyleneimine and glucose. Such as polymer P(GMA-MMA-DVB)-PG adsorption capacity up to 36.75 mg/g [15]. An inorganic boron adsorbent grafted with N-methyl-D-glucamine and glucose onto SiO_2 [2,16–18], the Si-MG adsorption capacity up to 16.65 mg/g. Such as glycidol-functionalized polymer and biopolymer adsorbents [19–22], including chitosan-based boron adsorption capacity of adsorbent CTS-MG of up to 35.13 mg/g [23]. In addition, ZIF-67 has an adsorption capacity of up to 579.80 mg/g depending on electrostatic adsorption and ligand exchange boron adsorbents [24]. These adsorbents have high adsorption capacity, but the intermediate product is expensive, a complex manufacturing process, adsorbents are toxic, not environmentally friendly, have a short cycle life, and cannot be applied in practice and industrialization. Therefore, there is a need to continue investigating boron adsorbents with high adsorption capacity, long lifetime, low-cost, and high selectivity.

In this paper, SBA-15, SBA-16 and MCM-41 molecular sieves were synthesized and tris(hydroxymethyl)methyl aminomethane (TRIS) was grafted onto SBA-15, SBA-16 and MCM-41, respectively. Then the TRIS were grafted onto three chloromethylated molecular sieves by solvent thermal method, and the three boron adsorbents SBA-15-TRIS, SBA-16-TRIS and MCM-41-TRIS were successfully synthesized. The effects of pH, initial boron concentration, and contact time on boron adsorption were systematically studied. The adsorption kinetics, isothermal adsorption, ion effect experiments and cycle life of adsorbents were also studied. And to investigate the effect of the same functional group on the boron adsorption of the same component (organosilicon material) of the matrix support but adsorbents with different structure, to determine the relationship between structure and activity. It is expected to be used for boron enrichment from salt lake brine.

2. Experimental

2.1. Materials and method of determination of boron

F127 (EO106PO70EO106, BASF), P123 (EO20PO70EO20, M_{av} = 5,800), tetraethyl orthosilicate (TEOS), cetyltrimethylammonium bromide (CTAB), 3-chloropropyltrimethoxysilane were supplied by Shanghai Macklin Biochemical Technology Co., Ltd., China. Tris(hydroxymethyl)methyl aminomethane (TRIS) was purchased from Aladdin Co., China. $NH_3·H_2O$, H_3BO_3, NaCl, $CaCl_2$ and $MgCl_2$ were of analytical purity grade and with reported purities of >99.0%, these reagents were obtained from Chemical Reagent Factory of Tianjin Zhiyuan Co., China. Double distilled water with conductance less than 1.5 μS/cm and pH of about 6.6 at 298.15 K was used for all experiments.

Boron analyses were performed by UV-Vis spectroscopy using azomethine-H method [25], azomethine-H (4-hydroxy-5-((2-hydroxybenzylidene)amino)naphthalene-2,7-disulfonic acid), acetic acid, ascorbic acid and EDTA-2Na were main reagents for the analysis of boron.

2.2. Preparation of SBA-15, SBA-16 and MCM-41

The synthesis of SBA-15 [12], SBA-16 [13] and MCM-41 [26] were carried out according to literature reports.

Synthesis of SBA-15: P123 (8 g) was added to 2 M HCl (90 g), and after stirring, 0.8 g of CTAB was added, stirring was continued for 0.5 h, then 23.2 g of TEOS was added, and then 30 g H_2O was added. Stir at 38°C for 20 h and then at 100°C for an additional 24 h to obtain SBA-15.

Synthesis of SBA-16: F127 (4 g) was dissolved in a mixed solution of deionized water (190 g) and HCl (8.3 g) at 45°C, and after stirring uniformly, 12.0 g N-butanol was added, stirring was continued for 1 h. After TEOS (20 g) was added dropwise, after continuous stirring for 24 h, obtained reaction liquid was transferred to a polytetrafluoroethylene-lined reaction vessel, and hydrothermally reacted at 100°C for 24 h. After the reaction is completed, filtered, washed, and dried. Finally, it was placed in a muffle furnace, heated to 550°C at a rate of 1°C/min, and calcined in an air atmosphere for 6 h to obtain mesoporous SBA-16.

Synthesis of MCM-41: 25% $NH_3·H_2O$ (205 mL) and of H_2O (270 mL) were stirred uniformly, and then CTAB (2 g) was added. After stirring uniformly, TEOS (10 mL) was slowly added dropwise, stirring was continued for 2 h, and the obtained white suspension emulsion was filtered washed and drying. Finally, the temperature was raised to 550°C at a rate of 1°C/min, and calcined in an air atmosphere for 6 h, and the obtained white powder was MCM-41.

2.3. Preparation of SBA-15-Cl, SBA-16-Cl and MCM-41-Cl

Add 3 g of SBA-15, SBA-16 and MCM-41 to 25 mL of toluene, respectively. And 5 mL of tris(hydroxymethyl)methyl aminomethane was added, respectively. The mixture was stirred at room temperature for 1 h, then transferred to 110°C for heating and reflux for 24 h. When the reaction was

complete, it was filtered, washed with ethanol and deionized water, and dried at 60°C for 12 h obtain SBA-15-Cl, SBA-16-Cl and MCM-41-Cl, respectively.

2.4. Preparation of SBA-15-TRIS, SBA-16-TRIS and MCM-41-TRIS

Add 3 g of SBA-15-Cl, SBA-16-Cl and MCM-41-Cl to 30 mL of *N,N*-dimethylformamide, respectively. Then add 4.5 g TRIS to the above three reaction systems, respectively. Magnetically stir at room temperature for 2 h, then transfer to a stainles steel reactor and heat at 105°C for 12 h. After the reaction was completed, filtered, washed with ethanol and deionized water, and dried to obtain SBA-15-TRIS, SBA-16-TRIS and MCM-41-TRIS, respectively.

The reactions used to prepare SBA-15-TRIS, SBA-16-TRIS and MCM-41-TRIS are illustrated in Fig. 1.

2.5. Physicochemical measurements

Infrared (IR) spectrum was taken with a Shimadzu IR Prestige-21 spectrophotometer. The surface morphology of SBA-15-TRIS, SBA-16-TRIS and MCM-41-TRIS were visualized by an scanning electron microscopy (SEM) (JEOL, JSM-5600V, Japan). The surface element analysis by X-ray photoelectron spectroscopy (XPS) (ESCALAB 250Xi, Thermo Fisher Scientific, United States). Material structure was determined by X-ray diffraction (XRD) (D8 Advance, Bruker, Germany). Particle-size distribution tested by Malvern laser particle size analyzer (Malvern, Mastersizer 3000, United Kingdom). The concentration of boron in the solution was gauged by applying ultraviolet and visible spectrophotometer (T6, Beijing Purkinje General Instrument Co., Ltd., China).

2.6. Boron adsorption experiments

To study the adsorption properties of SBA-15-TRIS, SBA-16-TRIS and MCM-41-TRIS for boron from boric acid aqueous solution. The effects of pH (4–10), initial concentration of boric acid (5–750 mg/L), adsorption time (5–240 min) and ionic (Na^+, Mg^{2+}, Ca^{2+} and Cl^-) on the adsorption properties of the adsorbents were discussed. In this study, 0.1 g of adsorbent was added to 25 mL of known concentration of boric acid, in the constant temperature oscillator and the shaking speed was 210 rpm at 30°C. The adsorption capacity (mg/g) was calculated from the $Q = (C_0 - C_e) V/M$, where C_0 and C_e (mg/L) are the initial and equilibrium concentration of boron in the solution, respectively. V is the volume of the solution (L) and M is the mass of SBA-15-TRIS, SBA-16-TRIS and MCM-41-TRIS (g).

3. Results and discussion

3.1. Characterization of SBA-15-TRIS, SBA-16-TRIS and MCM-41-TRIS

3.1.1. Fourier-transform infrared spectra analysis of adsorbents

The infrared spectra of SBA-15, SBA-16, MCM-41, SBA-15-Cl, SBA-16-Cl, MCM-41-Cl, SBA-15-TRIS, SBA-16-TRIS, and MCM-41-TRIS are shown in Fig. 2. It can be seen from the figure that there is a strong absorption peak at 3,460 cm^{-1}, which is attributed to the contraction vibration peak of the hydroxyl group on the TRIS, and the absorption peak at 2,692 cm^{-1} is attributed to C–H shrinkage vibration peak on (3-chloropropyl)trimethoxysilane. The two absorption bands at 1,630 and 1,440 cm^{-1} were attributed to the bending vibration of N–H, which proved that TRIS was successfully grafted with (3-chloropropyl)trimethoxysilane [18,27]. In addition, the peaks at 1,087 and 463 cm^{-1} are attributable to the Si–O–Si bending vibration [15]. The analysis of the above characteristic peaks indicates that SBA-15-TRIS, SBA-16-TRIS and MCM-41-TRIS were successfully synthesized. Fig. 2b shows the IR of the three adsorbents after adsorption of boron. The changes before
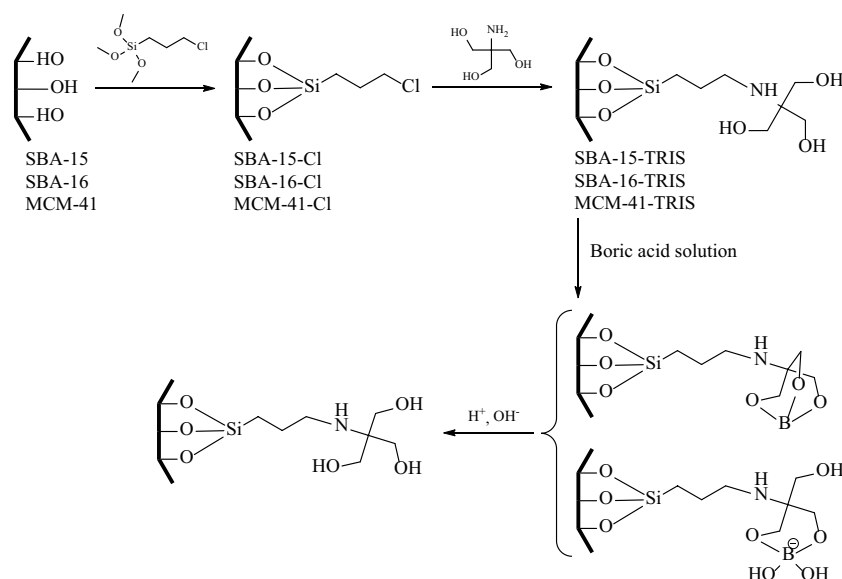

Fig. 1. Schematic representation of the synthesis of adsorbents.

and after adsorption can be seen. The red circled peak in the infrared image after adsorption becomes wider, which is due to the superposition of B–O (about 1,300 cm^{-1}) and B–OH (about 1,180 cm^{-1}) with Si–O (about 1,080 cm^{-1}) peaks.

3.1.2. SEM analysis of adsorbents

The surface morphology of SBA-15-TRIS, SBA-16-TRIS and MCM-41-TRIS was observed by scanning electron microscopy. It can be seen from Fig. 3 that SBA-15-TRIS has a spherical shape and a block shape, the particle size of the small ball is about 9 μm, and the size of the irregular block size distribution is different. SBA-16-TRIS is strip-shaped and irregularly shaped, and its particle size is distributed between nanometer and micrometer. MCM-41-TRIS is in the form of blocks, stripes, and irregular spheres stacked on top of each other, which are nano-sized spheres or blocks stacked on top of micron-sized ones.

3.1.3. Energy-dispersive X-ray and Mapping analysis of adsorbent

The mapping of SBA-16-TRIS is shown in Fig. 4. The results show that the adsorbent mainly contains C, O, N, and Cl elements. Indicating that TRIS and (3-chloropropyl) trimethoxysilane were successfully grafted onto SBA-16.

3.1.4. Particle size analysis

The particle-size distributions of SBA-15-TRIS, SBA-16-TRIS and MCM-41-TRIS were analyzed with a Malvern Laser Particle Size Analyzer. As can be seen from Fig. 5, the average particle size and particle-size distribution of SBA-15-TRIS, SBA-16-TRIS and MCM-41-TRIS are essentially the same and the particle sizes are below 60 μm. From the quantity distribution diagram, it can be seen that the particle size of SBA-15 clusters is within 10 μm. The reason for the inconsistency with the SEM analysis results is the difference between the overall particle-size distribution and the local analysis, but the results show that the three adsorbents have a narrow particle-size distribution and uniform size.

3.1.5. XRD analysis

The XRD patterns of SBA-15-TRIS, SBA-16-TRIS and MCM-41-TRIS are shown in Fig. 6. It can be seen from the XRD spectrum of of SBA-15-TRIS, SBA-16-TRIS and MCM-41-TRIS that there is obvious peak at 2θ = 22°. SiO$_2$ position and relative intensities of peak were confirmed with the standard XRD data from the Joint Committee on Powder Diffraction Standards (JCPDS-82-1558). In addition, the crystallinity of the three adsorbents is not very good due to the grafting of TRIS and (3-chloropropyl)trimethoxysilane,
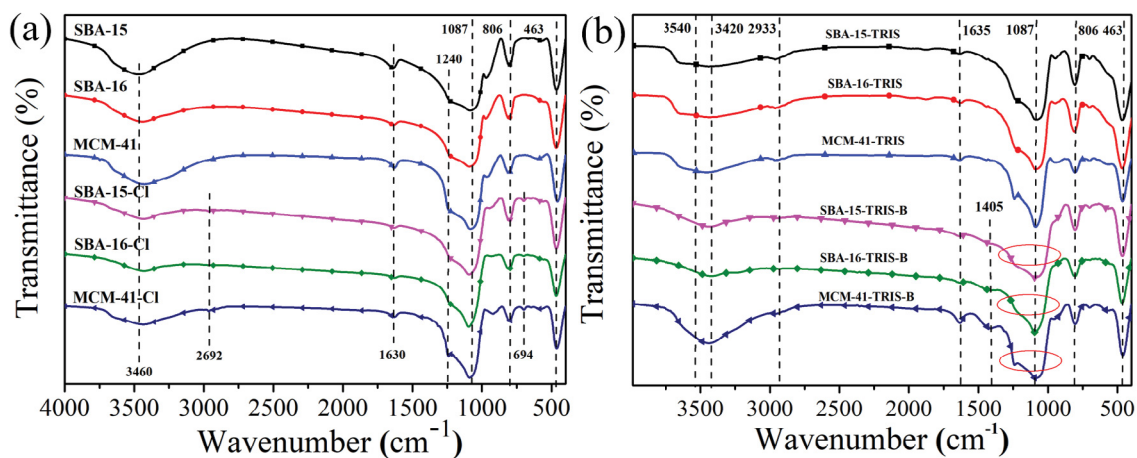

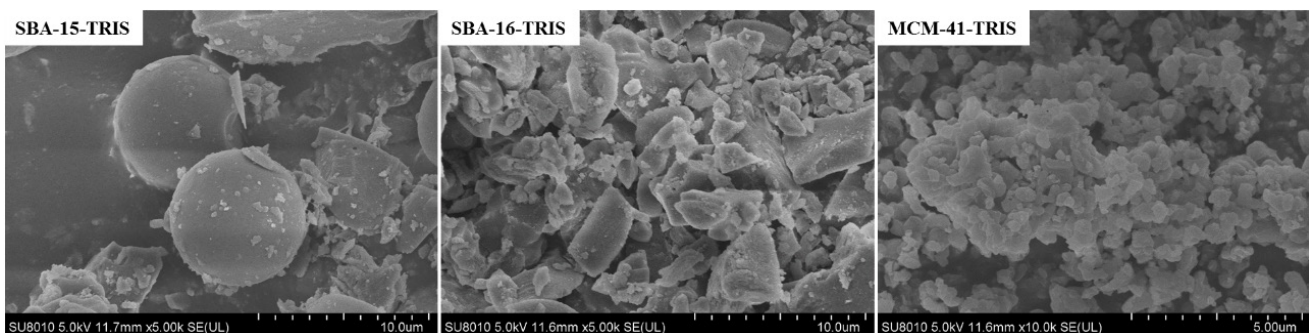Fig. 2. Fourier-transform infrared spectra of SBA-15-TRIS, SBA-16-TRIS and MCM-41-TRIS.

Fig. 3. SEM images for SBA-15-TRIS, SBA-16-TRIS and MCM-41-TRIS.

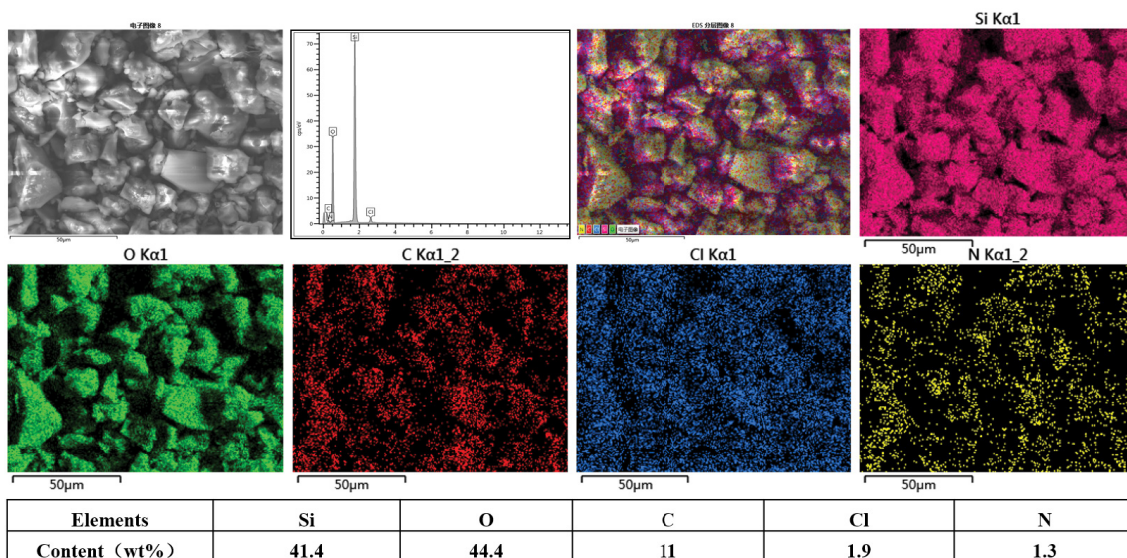| Elements	Si	O	C	Cl	N
Content（wt%）	41.4	44.4	11	1.9	1.3

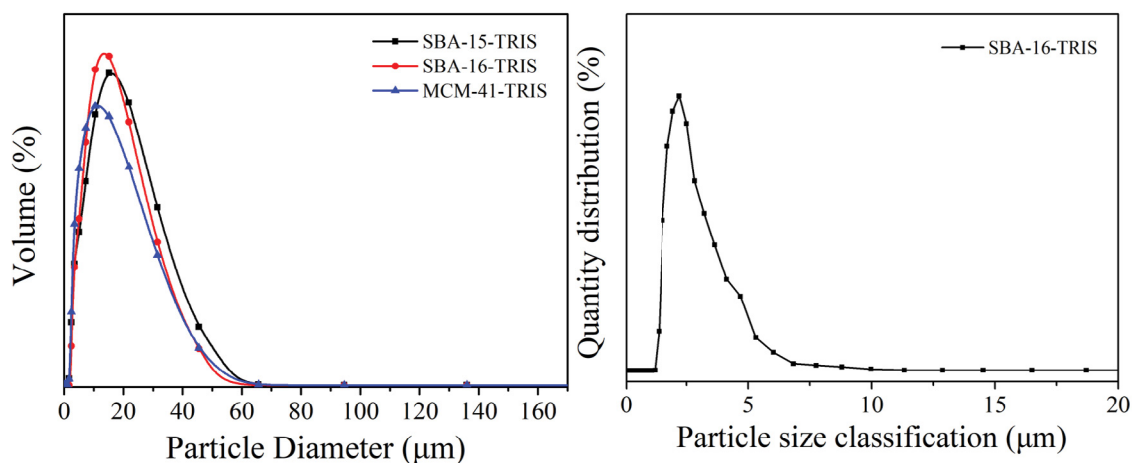Fig. 4. Elemental mapping analysis of the SBA-16-TRIS.

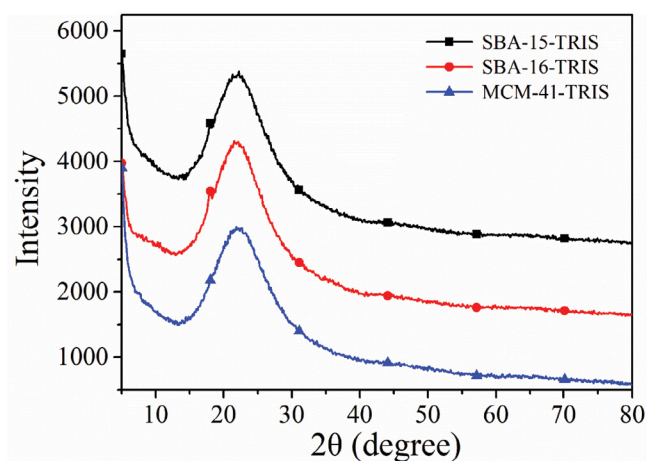Fig. 5. Particle-size distribution of the SBA-15-TRIS, SBA-16-TRIS and MCM-41-TRIS.

Fig. 6. XRD of adsorbents.

so these adsorbents show an amorphous structure, which is also the basic property of Si-based molecular sieves.

3.1.6. XPS analysis

The surface chemical composition of the adsorbent was analyzed by XPS, and the results are shown in Fig. 7. The results show the presence of C, O, N, Si, and B elements in MCM-41-TRIS after boron adsorption. The XPS peak of C1 belongs to C–C, C–OH and C–O–C on the adsorbent. In addition, after the reaction between the amino group of TRIS and MCM-41-Cl, TRIS was grafted onto MCM-41, so the N peak was observed at 398.6 eV. After MCM-41-TRIS adsorbed B, TRIS formed a chemical bond with B, so B peaks appeared at 190.7 and 191.5 eV, this is attributed to the B–O bond of $H_3BO_3/B(OH)_4^-$ and $B_3O_3(OH)_4^-/B_3O_3(OH)_5^{2-}$ [2]. The results show that the adsorbent successfully synthesized and adsorbed boron.
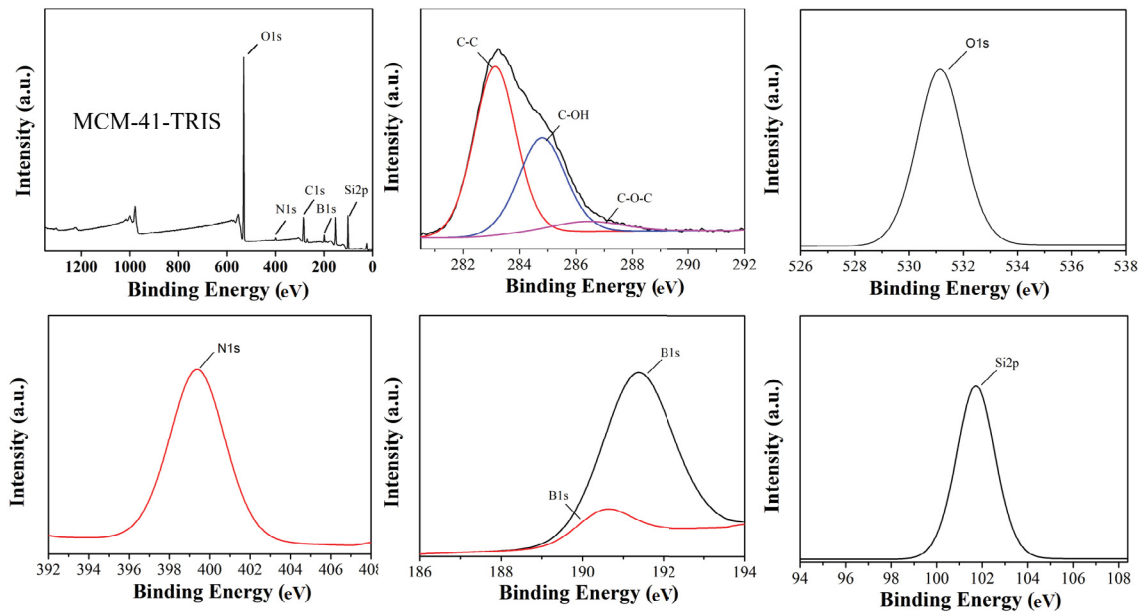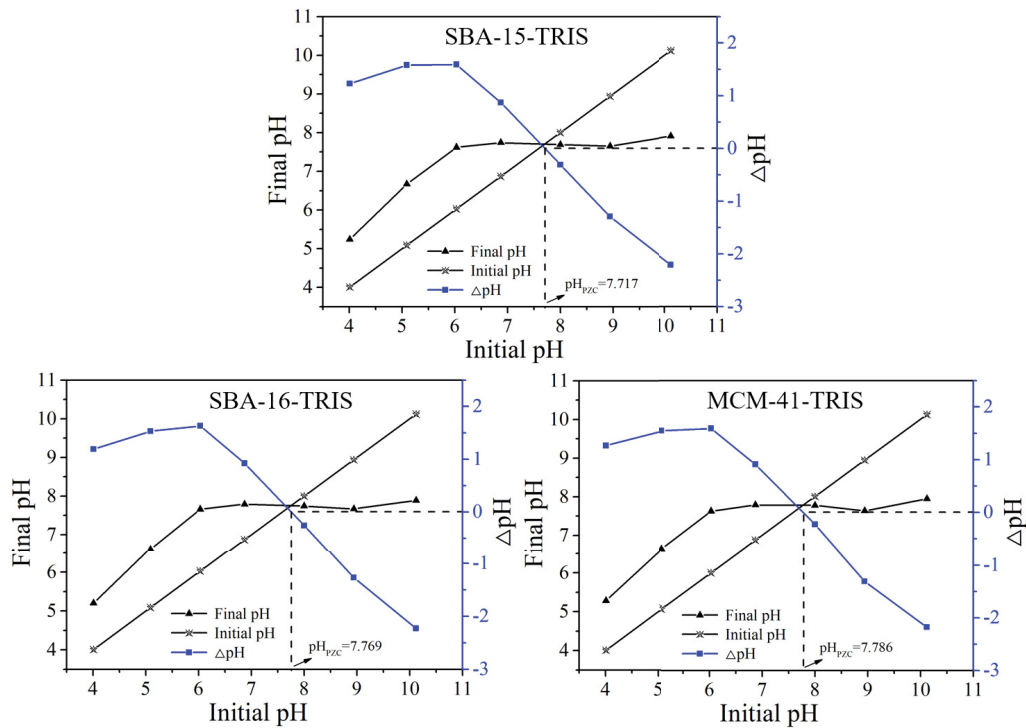
Fig. 7. XPS of MCM-41-TRIS adsorbent.

Fig. 8. Point of zero charge of adsorbents.

3.1.7. *Point of zero charge analysis of adsorbents*

The surface charge of the adsorbent directly affects the adsorption capacity of the adsorbent, and the surface hydroxyl groups of the adsorbent undergo protonation or deprotonation, so that the surface of the adsorbent becomes positively or negatively charged as the acid-base environment changes. It can be seen from Fig. 8 that the pH_{PZC} of SBA-15-TRIS, SBA-16-TRIS and MCM-41-TRIS are 7.717, 7.769 and 7.786, respectively. The surface of the adsorbent is positively charged when the solution pH is before pH_{PZC}, and the surface of the adsorbent is negatively charged when the pH of the solution is after pH_{PZC}.

3.2. Influence of experimental parameters

3.2.1. pH effect on the boron adsorption

The pH of the boric acid solution determines the distribution of $B(OH)_3$ and $B(OH)_4^-$ [28], which affects the adsorption capacity of the adsorbents at different pH values. As can be seen from Fig. 9, the adsorption performance of SBA-15-TRIS, SBA-16-TRIS and MCM-41-TRIS with pH 4 to 6 is greatly improved because the ability of polyols to complex with $B(OH)_3$ is weak under acidic conditions, with increasing pH, $B(OH)_3$ is continuously converted into and $B(OH)_4^-$, at this time different boron anions exist in the solution, $B(OH)_3$ and $B(OH)_4^-$ were adsorbed so that the adsorption amount further increased. When pH = 6–8, more polyborate and less metaborate is adsorbed by the adsorbent, so the amount of adsorption does not change much. At pH = 9, the maximum adsorption capacity of SBA-15-TRIS, SBA-16-TRIS and MCM-41-TRIS is due to the large amount of $B(OH)_3$ converted to $B(OH)_4^-$ and polyboron anions ($B_3O_3(OH)_4^-$ and $B_3O_3(OH)_5^{2-}$), they can form stable complexes with polyols, and boron in various forms can be adsorbed by the adsorbents so that the adsorption capacity reaches the maximum. At pH > 9, boron is converted into a large amount of $B(OH)_4^-$ and a large amount of OH$^-$ was generated [29], and the polyol on the surface of the adsorbents was protonated, causing the adsorbents to become negatively charged, and between the electrostatic repulsion occurs between polyol and $B(OH)_4^-$ and the reduction in complexation capacity leads to a decrease in adsorption capacity [11].

3.2.2. Adsorption isotherm

To better understand the adsorption process and mechanism, the effect of initial boric acid concentration on boron adsorption was studied. As shown in Fig. 10, as the boric acid concentration increased from 5–750 mg/L, the boric adsorption ability further increased, and finally reached an adsorption equilibrium. Because when boric acid is present in low concentrations the main form is $H_3BO_3/B(OH)_4^-$ [30], while at high concentrations $H_3BO_3/B(OH)_4^-$ and boric acid polymers ($B_3O_4(OH)$ and $B_3O_3(OH)_5^{2-}$) are present [31]. Therefore, various forms of boron anions are adsorbed by the adsorbent, so that the adsorption amount increases until the polyol active site is fully occupied and the adsorption capacity remains unchanged, the maximum adsorption capacities were 15.28, 15.70, and 14.17 mg/g, respectively. The boron adsorption performance of the three adsorbents is better than most of the adsorbents. The performance comparison with the adsorbents reported in the literature are summarized in Table 1. To further investigate the adsorption mechanism, Langmuir [Eq. (1)] and Freundlich [Eq. (2)] (Table 2) isotherm models were used to fit the experimental data. The fitted data are listed in Table 3. The results show that the Langmuir model is in better agreement with the adsorption process, indicating that the boron adsorption process of the three adsorbents is a
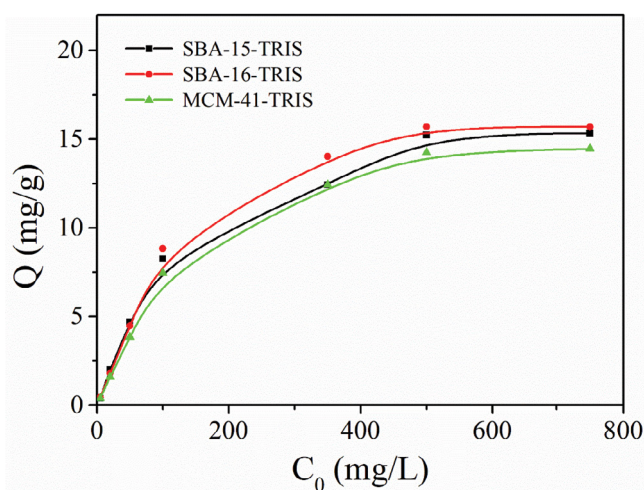

Fig. 10. Boron adsorption isotherms on SBA-15-TRIS, SBA-16-TRIS and MCM-41-TRIS.
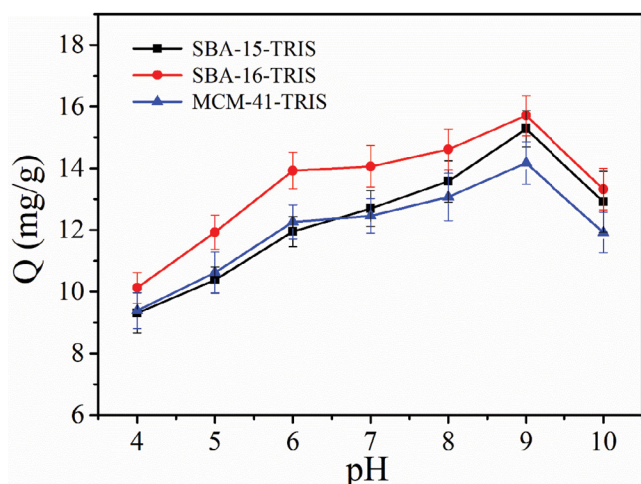

Fig. 9. Adsorption of boric acid by the adsorbents in the solution at different pH values.
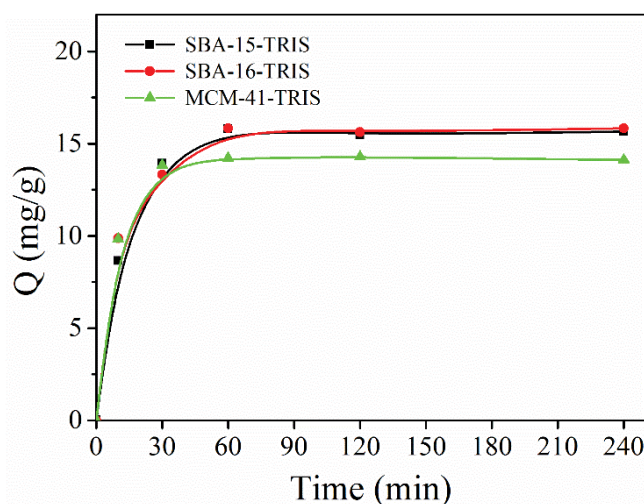

Fig. 11. Effect of contact time on the adsorption of boron (at 500 mg/L boron solution).

Table 1
Adsorption properties of the adsorbents reported in literature

No.	Adsorbents	Ligand	Q (mg/g)	T_e (min)	Solvent	References
1	SBA-15-GLC	Glucose	6.81	–	Xylene/methanol	[18]
	MCM-41-GLC	Glucose	2.70	–		
2	MCM-41-CL	Pyrocatechol	19.45	300	$CHCl_3$	[14]
	MCM-41-NACL	Nitropyrocatechol	16.73	300	Acetonitrile	
3	MCM-41-NMDG	NMDG	10.92	30	H_2O, $CHCl_3$	[34]
4	CA-KH-550-EPH	NMDG	15.35	600	DMF	[11]
5	PAN-PGMA	NMDG	5.5	100	DMF, THF	[35]
6	Si-MG	NMDG	16.65	120	DMF, Toluene	[2]
7	P(GMA-MMA-DVB)	NMDG	9.026		Toluene	[36]
		Glycidol	32.43	80	N-Methyl-2-pyrrolidone	[15]
8	PSF-*g*-PNMG	NMDG	2.09	110	Methanol, oxane	[37]
9	SBA-15-TRIS		15.28	60	Toluene	This work
	SBA-16-TRIS	TRIS	15.70	60	*N,N*-Dimethylformamide	
	MCM-41-TRIS		14.17	60		

Table 2
Adsorption kinetic models and adsorption isotherm models of boron [32]

Models			Parameters	
1	Langmuir adsorption isotherm		k_F	Freundlich adsorption constant
	$Q_e = \dfrac{Q_m k_L C_e}{1 + k_L C_e}$		n	Heterogeneity factor
			Q_e	Sorption amount at equilibrium (mg/g)
2	Freundlich adsorption isotherm		C_e	Equilibrium boric acid concentrations (mg/L)
	$\log Q_e = \log k_F + \dfrac{1}{n} \log C_e$		Q_m	Monolayer saturation adsorption (mg/g)
			k_L	Langmuir adsorption isotherm constant
3	Pseudo-first-order kinetics		Q_e	Sorption amounts at equilibrium
	$\ln(Q_e - Q_t) = \ln Q_e - k_1 t$		Q_t	Amount of boron adsorbed at time t
			k_1	Pseudo-first-order (min^{-1})
4	Pseudo-second-order		k_2	Pseudo-second-order rate constants (g mg^{-1} min^{-1})
	$\dfrac{t}{Q_t} = \dfrac{1}{k_2 Q_e^2} + \dfrac{t}{Q_e}$		R^2	R^2 that appears after the simulation refers to the correlation coefficient

Table 3
Fitting data of isotherm parameters for the boron adsorption of the adsorbents

Materials	Langmuir isotherm model			Freundlich isotherm model		
	Q_{max} (mg/g)	k_L (L/mg)	R^2	k_F	n	R^2
SBA-15-TRIS	19.57	0.0055	0.979	0.1963	1.3992	0.930
SBA-16-TRIS	20.28	0.0056	0.983	0.2036	1.3997	0.943
MCM-41-TRIS	19.01	0.0050	0.985	0.1702	1.3779	0.951

single molecular layer adsorption belonging to chemical adsorption [21].

3.2.3. Adsorption kinetics

The relationship between adsorption time and boron adsorption capacity is shown in Fig. 11. The adsorption capacity of SBA-15-TRIS, SBA-16-TRIS and MCM-41-TRIS increased rapidly within 30 min and then gradually equalized the adsorption capacity remained unchanged at 60 min, indicating that boron is the adsorption site of the three adsorbents took completely. To further understand the adsorption mechanism and the adsorption process, the experimental data were fitted using kinetic models (Table 2), pseudo-first-order kinetic models [Eq. (3)] and pseudo-second-order kinetic models [Eq. (4)] [33] Fitted with

results in Table 4, according to the correlation coefficient R^2, it shows that the pseudo-second-order kinetic model is more consistent with the adsorption kinetics, which proves that chemical adsorption dominates the adsorption process [20], The results show that there is a chemical combination between boron and three adsorbents.

3.2.4. Effect of ionic strength

When the initial concentration of boron was kept at 500 mg/L, the adsorption of boron by three adsorbents was
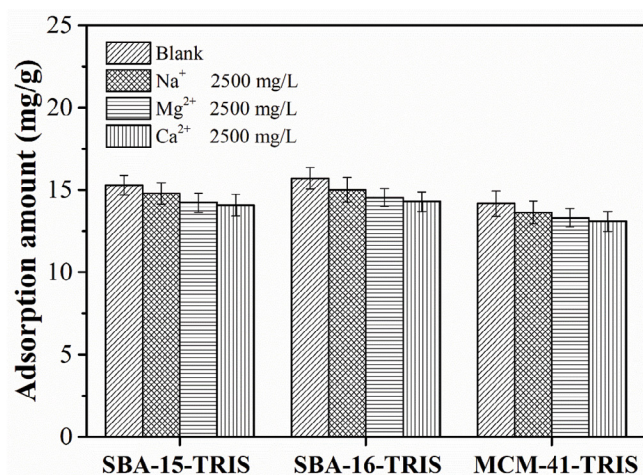

Fig. 12. Effect of co-ions under on the adsorption.

studied by adding 2,500 mg/L of Na^+, Mg^{2+} and Ca^{2+} (ignoring Cl^-). As shown in Fig. 12, the adsorption of boron by SBA-15-TRIS, SBA-16-TRIS and MCM-41-TRIS was almost unaffected in the presence of interfering ions. Na^+, Mg^{2+}, Ca^{2+}, and Cl^- hardly compete with boron in adsorption. The results show that the three adsorbents have strong ability to resist ion interference.

3.2.5. Regeneration of adsorbents

The recyclability of adsorbents is important for industrial applications and cost control. The adsorption–desorption experiments of SBA-15-TRIS, SBA-16-TRIS and MCM-41-TRIS are as follows: add 1 mol/L HCl to the adsorbent after boron adsorption, then shake, and update the hydrochloric acid solution every 2 h. After three cycles, add 0.5 mol/L NaOH to neutralize, and wash with deionized water and filtered and dried. After five adsorption–desorption cycles, the adsorption situation is shown in Fig. 13 that the adsorption capacity of the three adsorbents still maintained more than 90% of the original capacity, indicating that the adsorbents have good life and stability.

3.2.6. Dissolution rate and IR of adsorbent

The dissolution loss rate of the SBA-16-TRIS after adsorption–desorption 10 times is very low (0.93%), and the IR before and after the adsorption of the adsorbent remains essentially unchanged (Fig. 14). The results show that the adsorbent has good stability.
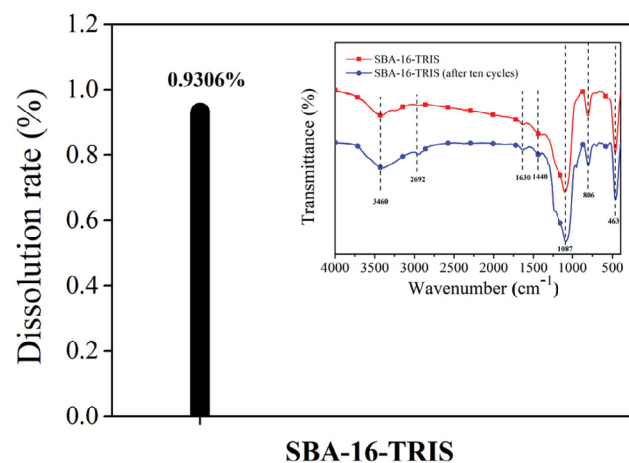
Table 4
Kinetic parameters for boron adsorption

Materials	T (°C)	First-order model fitting			Second-order model fitting		
		$Q_{e,cal}$ (mg/g)	k_1	R^2	$Q_{e,cal}$ (mg/g)	k_2	R^2
SBA-15-TRIS		9.34	0.0299	0.907	15.95	0.0143	0.999
SBA-16-TRIS	30	13.24	0.0638	0.958	15.60	0.0330	0.999
MCM-41-TRIS		11.57	0.0907	0.978	14.66	0.0182	0.999
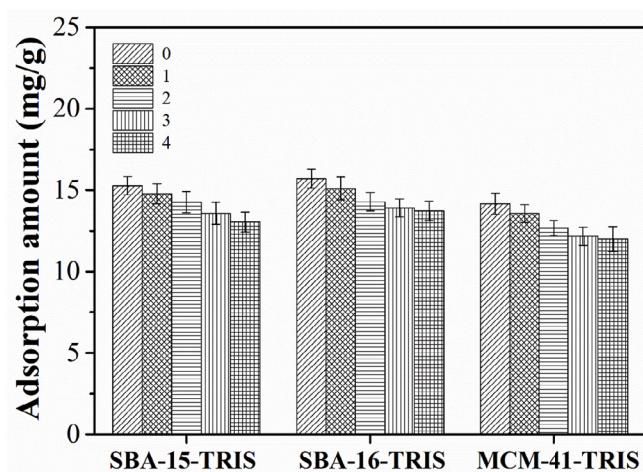
Fig. 13. Recycling of prepared resins for boron adsorption.

Fig. 14. Dissolution rate and IR of adsorbent.

4. Conclusions

TRIS-functionalized mesoporous SBA-15, SBA-16, and MCM-41 were synthesized and their boron adsorption properties studied. The three TRIS-functionalized molecular sieve adsorbents have good adsorption performance and have the strongest adsorption capacity at pH = 9. And the same functional group has little influence on the boron adsorption capacity of different carrier adsorbents of the same type (organosilicon material). The boron adsorption process of the three adsorbents is better suited to describe the Langmuir adsorption isotherm model and the pseudo-second-order kinetic model. Their adsorption of boron is a process of monolayer adsorption and chemisorption. Na$^+$, Mg^{2+}, Ca^{2+}, and Cl$^-$ ions have little effect on boron adsorption. In addition, the adsorbents maintain a good lifetime after five adsorption–desorption cycles. Therefore, it can be assumed that the adsorption of boron by the TRIS-modified mesoporous silicas SBA-15, SBA-16 and MCM-41 from the boron-containing salt lake brine has a certain application potential.

Declaration of interests

The authors declare that they have no known competing financial interests or personal relationships that could have appeared to influence the work reported in this paper.

CRediT authorship contribution statement

Qinglong Luo: Implementation, data analysis, draft. Lei Liu, Ruiqiang Dong, Mingzhe Dong and Zhongfu Cheng: Validation. Visualization, Jun Li and Zhijian Wu: Supervision. Xueli Huang: Conceptualization, Methodology and Supervision.

Acknowledgement

References

[1]   B. Wang, X. Guo, P. Bai, Removal technology of boron dissolved in aqueous solutions – a review, Colloids Surf., A, 444 (2014) 338–344.
[2]   L. Xu, Y. Liu, H. Hu, Z. Wu, Q. Chen, Synthesis, characterization and application of a novel silica based adsorbent for boron removal, Desalination, 294 (2012) 1–7.
[3]   L. Melnyk, V. Goncharuk, I. Butnyk, E. Tsapiuk, Boron removal from natural and wastewaters using combined sorption/membrane process, Desalination, 185 (2005) 147–157.
[4]   M.M. Nasef, M. Nallappan, Z. Ujang, Polymer-based chelating adsorbents for the selective removal of boron from water and wastewater: a review, React. Funct. Polym., 85 (2014) 54–68.
[5]   Z. Guan, J. Lv, P. Bai, X. Guo, Boron removal from aqueous solutions by adsorption – a review, Desalination, 383 (2016) 29–37.
[6]   L.A. Melnik, Y.V. Babak, V.V. Goncharuk, I.K. Chepurnaya, Application potential of boron-selective sorbents of different nature for water conditioning in terms of the boron content, J. Water Chem. Technol., 37 (2015) 25–31.
[7]   E. Yoshikawa, A. Sasaki, M. Endo, Removal of boron from wastewater by the hydroxyapatite formation reaction using acceleration effect of ammonia, J. Hazard. Mater., 237–238 (2012) 277–282.
[8]   N. Zhang, J. Lyu, P. Bai, X. Guo, Boron isotopic separation with pyrocatechol-modified resin by chromatography technology: experiment and numerical simulation, J. Ind. Eng. Chem., 57 (2018) 244–253.
[9]   N. Hilal, G.J. Kim, C. Somerfield, Boron removal from saline water: a comprehensive review, Desalination, 273 (2011) 23–35.
[10]   J.G. Neo, S. Japip, L. Luo, T.S. Chung, M. Weber, C. Maletzko, Hydroxyl-terminated poly(ethyleneimine) polymer enhanced ultrafiltration for boron removal, Sep. Purif. Technol., 222 (2019) 214–220.
[11]   L. Sun, J. Huang, H. Liu, Y. Zhang, X. Ye, H. Zhang, A. Wu, Z. Wu, Adsorption of boron by CA@KH-550@EPH@NMDG (CKEN) with biomass carbonaceous aerogels as substrate, J. Hazard. Mater., 358 (2018) 10–19.
[12]   T.M. Albayati, A.M. Doyle, Encapsulated heterogeneous base catalysts onto SBA-15 nanoporous material as highly active catalysts in the transesterification of sunflower oil to biodiesel, J. Nanopart. Res., 17 (2015) 109, doi: 10.1007/s11051-015-2924-6.
[13]   W.J.J. Stevens, M. Mertens, S. Mullens, I. Thijs, G. Van Tendeloo, P. Cool, E.F. Vansant, Formation mechanism of SBA-16 spheres and control of their dimensions, Microporous Mesoporous Mater., 93 (2006) 119–124.
[14]   Y. Chen, J. Lyu, Y. Wang, T. Chen, Y. Tian, P. Bai, X. Guo, Synthesis, characterization, adsorption, and isotopic separation studies of pyrocatechol-modified MCM-41 for efficient boron removal, Ind. Eng. Chem. Res., 58 (2019) 3282–3292.
[15]   B.F. Senkal, N. Bicak, Polymer supported iminodipropylene glycol functions for removal of boron, React. Funct. Polym., 55 (2003) 27–33.
[16]   C. Sanfeliu, R. Martínez-Máñez, F. Sancenón, J. Soto, P. Amorós, T. Azaïs, M.D. Marcos, ^{11}B-MAS NMR approach to the boron adsorption mechanism on a glucose-functionalised mesoporous silica matrix, Microporous Mesoporous Mater., 266 (2018) 232–241.
[17]   B. Tural, Separation and preconcentration of boron with a glucamine modified novel magnetic sorbent, Clean (Weinh), 38 (2010) 321–327.
[18]   L. Wang, T. Qi, Y. Zhang, Novel organic-inorganic hybrid mesoporous materials for boron adsorption, Colloids Surf., A, 275 (2006) 73–78.
[19]   Z. Wang, Z. Wu, Y. Zhang, J. Meng, Hyperbranched-polyol-tethered poly (amic acid) electrospun nanofiber membrane with ultrahigh adsorption capacity for boron removal, Appl. Surf. Sci., 402 (2017) 21–30.
[20]   X. Du, J. Meng, R. Xu, Q. Shi, Y. Zhang, Polyol-grafted polysulfone membranes for boron removal: effects of the ligand structure, J. Membr. Sci., 476 (2015) 205–215.
[21]   J. Meng, J. Cao, R. Xu, Z. Wang, R. Sun, Hyperbranched grafting enabling simultaneous enhancement of the boric acid uptake and the adsorption rate of a complexing membrane, J. Mater. Chem. A, 4 (2016) 11656–11665.
[22]   M.R. Kotte, M. Cho, M.S. Diallo, A facile route to the preparation of mixed matrix polyvinylidene fluoride membranes with in-situ generated polyethyleneimine particles, J. Membr. Sci., 450 (2014) 93–102.
[23]   Y.T. Wei, Y.M. Zheng, J.P. Chen, Design and fabrication of an innovative and environmental friendly adsorbent for boron removal, Water Res., 45 (2011) 2297–2305.
[24]   J. Zhang, Y. Cai, K. Liu, Extremely effective boron removal from water by stable metal organic framework ZIF-67, Ind. Eng. Chem. Res., 58 (2019) 4199–4207.
[25]   Ş. Sungur, R. Okur, Using azomethine-H method determination of boron contents of various foods consumed in Hatay Region in Turkey, Food Chem., 115 (2009) 711–714.

[26] S.M. Alardhi, T.M. Albayati, J.M. Alrubaye, A hybrid adsorption membrane process for removal of dye from synthetic and actual wastewater, Chem. Eng. Process., 157 (2020) 108113, doi: 10.1016/j.cep.2020.108113.

[27] L.Z. Fekri, M. Nikpassand, S. Pourmirzajani, B. Aghazadeh, Synthesis and characterization of amino glucose-functionalized silica-coated NiFe$_2$O$_4$ nanoparticles: a heterogeneous, new and magnetically separable catalyst for the solvent-free synthesis of pyrano[3,2-*c*]chromen-5(4*H*)-ones, RSC Adv., 8 (2018) 22313–22320.

[28] C.G. Salentine, High-field boron-[11]NMR of alkali borates. Aqueous polyborate equilibria, Inorg. Chem., 22 (1983) 3920–3924.

[29] H. Liu, X. Ye, Q. Li, T. Kim, B. Qing, M. Guo, F. Ge, Z. Wu, K. Lee, Boron adsorption using a new boron-selective hybrid gel and the commercial resin D564, Colloids Surf., A, 341 (2009) 118–126.

[30] F.G.A. Stone, Boron, metallo-boron compounds and boranes, J. Electroanal. Chem., 9 (1965) 488, doi: 10.1016/0022-0728(65)85051-3.

[31] C.L. Christ, A.H. Truesdell, R.C. Erd, Borate mineral assemblages in the system Na$_2$O-CaO-MgO-B$_2$O$_3$-H$_2$O, Geochim. Cosmochim. Acta, 31 (1967) 313–337.

[32] Q. Luo, L. He, X. Wang, H. Huang, X. Wang, S. Sang, X. Huang, Cyclodextrin derivatives used for the separation of boron and the removal of organic pollutants, Sci. Total Environ., 749 (2020) 141487, doi: 10.1016/j.scitotenv.2020.141487.

[33] Q. Wu, M. Liu, X. Wang, A novel chitosan based adsorbent for boron separation, Sep. Purif. Technol., 211 (2019) 162–169.

[34] Ö. Kaftan, M. Açikel, A.E. Eroğlu, T. Shahwan, L. Artok, C. Ni, Synthesis, characterization and application of a novel sorbent, glucamine-modified MCM-41, for the removal/preconcentration of boron from waters, Anal. Chim. Acta, 547 (2005) 31–41.

[35] J. Wang, T. Wang, L. Li, P. Wu, K. Pan, B. Cao, Functionalization of polyacrylonitrile nanofiber using ATRP method for boric acid removal from aqueous solution, J. Water Process Eng., 3 (2014) 98–104.

[36] N. Biçak, N. Bulutçu, B.F. Şenkal, M. Gazi, Modification of crosslinked glycidyl methacrylate-based polymers for boron-specific column extraction, React. Funct. Polym., 47 (2001) 175–184.

[37] Q. Shi, J.Q. Meng, R.S. Xu, X.L. Du, Y.F. Zhang, Synthesis of hydrophilic polysulfone membranes having antifouling and boron adsorption properties via blending with an amphiphilic graft glycopolymer, J. Membr. Sci., 444 (2013) 50–59.